Chapter 5

New Insights into the Bonding of Transition Metals with Phosphine and N-Heterocyclic Carbene Ligands: Implications for the Activity of Ruthenium Olefin Metathesis Catalysts

> On a commuter train to London there were two passengers who always caught the train at the same time, and who often sat across from one another. One of the passengers had a pad of paper and kept throwing a sheet out the window during the ride. After some days of seeing this, the other passenger asked, "Why are you doing this?" His answer was "To keep the lions away." The questioner said, "But there are no lions in England," and the response was, "Yes, so you see it works."[1]

Introduction

The coordination chemistry of phosphine ligands was pioneered by Mann, Chatt, and others beginning in the 1930s,[2] and currently phosphines are one of the most important classes of L-type ancillary ligands in inorganic chemistry. Particularly because of their applications in a wide range of synthetically and catalytically valuable transition metal systems, there have been numerous efforts to understand the stereoelectronic properties of phosphine ligands and the nature

---

1. Story attributed to Joseph Chatt by Basolo, F. "Mechanisms of Platinum Reactions." In *Modern Coordination Chemistry: The Legacy of Joseph Chatt*. Leigh, G. J., Winterton, N., Eds. Royal Society of Chemistry: Cambridge, 2002, pp. 326.
2. (a) *Modern Coordination Chemistry: The Legacy of Joseph Chatt*; Leigh, G. J., Winterton, N., Eds.; Royal Society of Chemistry: Cambridge, 2002. (b) Levason, W. In *The Chemistry of Organophosphorus Compounds, Volume 1*; Hartley, F. R., Ed.; John Wiley & Sons: 1990; chapter 15.

of metal–phosphine bonding.[3] Although the basic bonding scheme has been well established, many of the details remain elusive and are often debated in the literature.[3]

In general, the properties of a metal complex can be probed in a variety of ways, and each of these provides information about different aspects of catalyst behavior. For example, typical substrate–catalyst activity studies provide valuable insight with regard to synthetic scope, and kinetic studies reveal the mechanistic details of reaction pathways. However, neither of these approaches yields direct information about the geometric or electronic structure of the catalyst complex. This fundamental knowledge is essential for understanding the origins of chemical and physical properties, and it can be used together with activity and mechanistic data to approach the ultimate goal of predicting catalytic performance *a priori*.

Our particular interest is the ruthenium alkylidene catalysts commonly employed in olefin metathesis reactions. The two most widely used derivatives are $(PCy_3)_2(Cl)_2Ru{=}CHPh$ (**5.1**) and $(H_2IMes)(PCy_3)(Cl)_2Ru{=}CHPh$ (**5.2**), due to their favorable activity and stability profiles.[4] Both catalysts contain strongly electron-donating and sterically bulky ancillary ligands, tricyclohexylphosphine (PCy_3) in **5.1** and the N-heterocyclic carbene H_2IMes (1,3-dimesityl-imidazolidine-2-ylidene) in **5.2**.

Extensive substrate–catalyst activity studies have established that catalyst **5.2** is more active than **5.1** in olefin metathesis reactions.[4,5] Kinetic studies and phosphine exchange experiments have revealed that the general mechanism involves initial phosphine dissociation from the 16-electron precatalyst $(L)(PR_3)(Cl)_2Ru{=}CHR'$ (L = PCy_3 or H_2IMes) to generate a 14-electron intermediate $(L)(Cl)_2Ru{=}CHR'$, which then coordinates to an olefin and enters the propagating metathesis cycle (Figure 5.1).[6] However, catalysts **5.1** and **5.2** have dramatically different initiation and propagation rates. For example, **5.1** initiates at a rate (k_1) approximately two orders of magnitude faster than **5.2**. On the other hand, the ratio of rates for entry into the catalytic cycle versus phosphine rebinding (k_{-1}/k_2) is four orders of magnitude less for **5.1** than

---

3. Reviews: (a) Song, S.; Alyea, E. C. *Comments Inorg. Chem.* **1996**, *18*, 145-164. (b) Alyea, E. C.; Song, S. *Comments Inorg. Chem.* **1996**, *18*, 189-221. (c) Dias, P. B.; Minas de Piedade, M. E.; Martinho Simões, J. A. *Coord. Chem. Rev.* **1994**, *135/136*, 737-807. (d) Tolman, C. A. *Chem. Rev.* **1977**, *77*, 313-348.
4. (a) Trnka, T. M.; Grubbs, R. H. *Acc. Chem. Res.* **2001**, *34*, 18-29. (b) Scholl, M.; Ding, S.; Lee, C. W.; Grubbs, R. H. *Org. Lett.* **1999**, *1*, 953-956. (c) Schwab, P.; Grubbs, R. H.; Ziller, J. W. *J. Am. Chem. Soc.* **1996**, *118*, 100-110. (d) Schwab, P.; France, M. B.; Ziller, J. W.; Grubbs, R. H. *Angew. Chem., Int. Ed. Engl.* **1995**, *34*, 2039-2041.
5. (a) Mol, J. C. *Green Chem.* **2002**, *4*, 5-13. (b) Fürstner, A.; Ackermann, L.; Gabor, B.; Goddard, R.; Lehmann, C. W.; Mynott, R.; Stelzer, F.; Thiel, O. R. *Chem. Eur. J.* **2001**, *7*, 3236-3253.
6. (a) Sanford, M. S.; Ulman, M.; Grubbs, R. H. *J. Am. Chem. Soc.* **2001**, *123*, 749-750. (b) Sanford, M. S., Love, J. A., Grubbs, R. H. *J. Am. Chem. Soc.* **2001**, *123*, 6543-6554. (c) Adlhart, C.; Hinderling, C.; Baumann, H.; Chen, P. *J. Am. Chem. Soc.* **2000**, *122*, 8204-8214. (d) Hinderling, C.; Adlhart, C.; Chen, P. *Angew. Chem., Int. Ed. Engl.* **1998**, *37*, 2685-2689. (e) Dias, E. L.; Nguyen, S. T.; Grubbs, R. H. *J. Am. Chem. Soc.* **1997**, *119*, 3887-3897.

5.2. Speculation about the stereoelectronic basis of these effects abounds, but in this study, we provide experimental evidence relating to the nature of metal–phosphine and metal–N-heterocyclic carbene bonding. The questions we seek to answer are as follows: *why* does **5.1** initiate more readily than **5.2**, and *why* does **5.1** propagate more slowly than **5.2**?

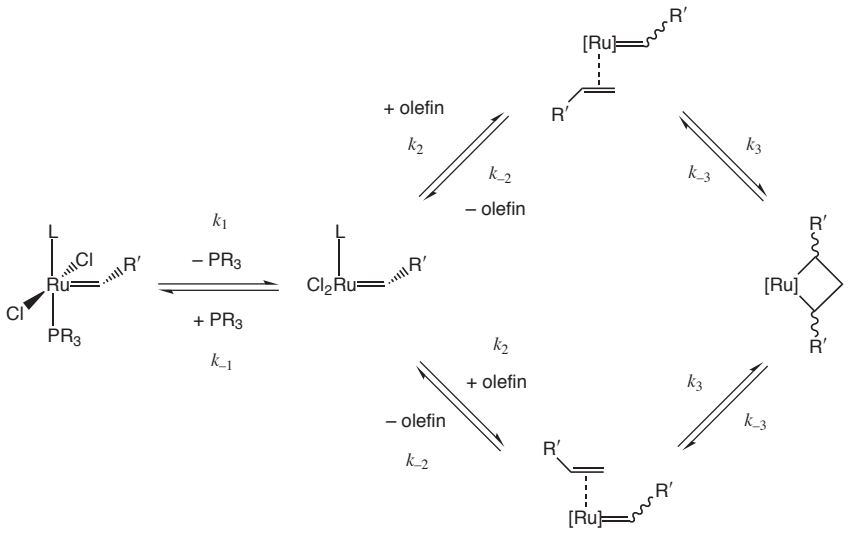

Figure 5.1

To address these questions, we have studied several series of model complexes, including $(CO)_5Mo(L)$, Cp*Ru(Cl)(L), and Cp*Ru(Cl)(CO)(L), where L is a N-heterocyclic carbene (NHC), phosphine, or tertiary amine ligand. Although it may seem more straightforward to study **5.1** and **5.2** directly, this approach was not feasible for multiple reasons. For instance, these ruthenium alkylidene complexes do not contain many spectroscopic handles; they are too complex to be studied by some techniques (*e.g.*, ultrafast electron diffraction);[7] and they are not stable to other techniques (*e.g.*, gas-phase photoelectron spectroscopy).[8] In comparison, $(CO)_5Mo(L)$ complexes have numerous spectroscopic handles and high symmetry, which simplifies the analysis of molecular orbital interactions. There is also a wealth of useful information on $(CO)_5Mo(L)$ complexes in the literature, including data from ^{13}C and ^{31}P NMR

7. Ihee, H.; Cao, J.; Zewail, A. H. *Angew. Chem., Int. Ed.* **2001**, *40*, 1532-1536.
8. Complexes **5.1** and **5.2** are not stable under the conditions required for gas-phase photoelectron spectroscopy. In both cases, only free PCy_3 is observed, which is consistent with PCy_3 dissociation in solution (see reference 6a-b).

spectroscopy,[9] IR and Raman spectroscopy,[10] x-ray crystallography,[11] photoelectron spectroscopy,[12] kinetics,[13] and theoretical studies.[14] The choice of molybdenum instead of chromium or tungsten was based on the opportunity to use ^{95}Mo NMR spectroscopy, which has been applied previously to the $(CO)_5Mo(L)$ system.[15] In addition, Cp*Ru(Cl)(L) and Cp*Ru(Cl)(CO)(L) complexes are readily synthesized, and the electronic structure of Cp* derivatives has been studied extensively.

N-heterocyclic carbenes are related to phosphines because of their applications as ancillary ligands for a wide variety of metal complexes, and because of their similar bonding mode (L-type, $2e^-$ donor ligand). In addition to their applications in olefin metathesis, NHC-coordinated complexes have been used successfully in Heck and Suzuki couplings, aryl amination, hydrogenation, hydroformylation, and many other catalytic systems.[16,17]

---

9. Examples: (a) Bodner, G. M.; May, M. P.; McKinney, L. E. *Inorg. Chem.* **1980**, *19*, 1951-1958. (b) Guns, M. F.; Claeys, E. G.; van der Kelen, G. P. *J. Mol. Struct.* **1979**, *54*, 101-109. (c) Grim, S. O.; Wheatland, D. A.; McFarlane, W. *J. Am. Chem. Soc.* **1967**, *89*, 5573-5577.
10. Examples: (a) Aroney, M. J.; Davies, M. S.; Hambley, T. W.; Pierens, R. K. *J. Chem. Soc., Dalton Trans.* **1994**, 91-96. (b) Davies, M. S.; Allen, G. W.; Aroney, M. J.; Hambley, T. W.; Pierens, R. K. *J. Mol. Struct.* **1994**, *326*, 81-91. (c) Davies, M. S.; Pierens, R. K.; Aroney, M. J. *J. Organomet. Chem.* **1993**, *458*, 141-146. (d) Aroney, M. J.; Clarkson, R. M.; Hambley, T. W.; Pierens, R. K. *J. Organomet. Chem.* **1992**, *426*, 331-342. (e) Denham, E. L.; Clark, R. J. *J. Chromatography* **1984**, *301*, 253-260. (f) Koelle, U. *J. Organomet. Chem.* **1977**, *133*, 53-58. (g) Darensbourg, D. J.; Brown, T. L. *Inorg. Chem.* **1968**, *7*, 959-966. (h) Darensbourg, D. J.; Brown, T. L. *Inorg. Chem.* **1968**, *7*, 959-966. (i) Cotton, F. A. *Inorg. Chem.* **1964**, *3*, 702-711. (j) Kraihanzel, C. S.; Cotton, F. A. *Inorg. Chem.* **1963**, *2*, 533-540. (k) Cotton, F. A.; Kraihanzel, C. S. *J. Am. Chem. Soc.* **1962**, *84*, 4432-4438.
11. Examples: (a) Frenking, G.; Wichmann, K.; Fröhlich, N.; Grobe, J.; Golla, W.; Le Van, D.; Krebs, B.; Läge, M. *Organometallics* **2002**, *21*, 2921-2930. (b) Cortes-Figueroa, J. E.; Leon-Velazquez, M. S.; Ramos, J.; Jasinski, J. P.; Deene, D. A.; Zubkowski, J. D.; Valente, E. J. *Acta Cryst.* **2000**, *C56*, 1435-1437. (c) Liu, C.-Y.; Chen, D.-Y.; Lee, G.-H.; Peng, S.-M.; Liu, S.-T. *Organometallics* **1996**, *15*, 1055-1061. (d) Davies, M. S.; Aroney, M. J.; Buys, I. E.; Hambley, T. W.; Calvert, J. L. *Inorg. Chem.* **1995**, *34*, 330-336. (e) Dunbar, K. R.; Sun, J.-S.; Haefner, S. C.; Matonic, J. H. *Organometallics* **1994**, *13*, 2713-2720. (f) Aroney, M. J.; Buys, I. E.; Davies, M. S.; Hambley, T. W. *J. Chem. Soc., Dalton Trans.* **1994**, 2827-2834. (g) Cotton, F. A.; Darensbourg, D. J.; Ilsley, W. H. *Inorg. Chem.* **1981**, *20*, 578-583.
12. (a) Lichtenberger, D. L.; Jatcko, M. E. *Inorg. Chem.* **1992**, *31*, 451-455. (b) Lichtenberger, D. L.; Kellogg, G. E.; Landis, G. H. *J. Chem. Phys.* **1985**, *83*, 2759-2768. (c) Bursten, B. E.; Darensbourg, D. J.; Kellogg, G. E.; Lichtenberger, D. L. *Inorg. Chem.* **1984**, *23*, 4361-4365. (d) Yarbrough, L. W.; Hall, M. B. *Inorg. Chem.* **1978**, *8*, 2269-2275.
13. Gao, Y.-C.; Shi, Q.-S.; Kershner, D. L.; Basolo, F. *Inorg. Chem.* **1988**, *27*, 188-191.
14. (a) Frenking, G.; Dapprich, S.; Meisterknecht, T.; Uddin, J. In *Metal-Ligand Interactions in Chemistry, Physics and Biology*; Russo, N., Salahub, D. R., Eds.; Kluwer Academic: Norwell, MA, 2000; pp. 73-89. (b) van Wüllen, C. *J. Comp. Chem.* **1997**, *18*, 1985-1992.
15. (a) Alyea, E. C.; Song, S. *Inorg. Chem.* **1995**, *34*, 3864-3873. (b) Alyea, E. C.; Somogyvari, A. *Trans. Met. Chem.* **1987**, *12*, 310-314. (c) Masters, A. F.; Bossard, G. E.; George, T. A.; Brownlee, R. T. C.; O'Connor, M. J.; Wedd, A. G. *Inorg. Chem.* **1983**, *22*, 908-911. (d) Gray, G. M.; Gray, R. J. *Organometallics* **1983**, *2*, 1026-1031. (e) Alyea, E. C.; Lenkinski, R. E.; Somogyvari, A. *Polyhedron* **1982**, *1*, 130-132. (f) Jaitner, P.; Wohlgenannt, W. *Monatshefte Chem.* **1982**, *113*, 699-703. (g) Bailey, J. T.; Clark, R. J.; Levy, G. C. *Inorg. Chem.* **1982**, *21*, 2085-2087. (h) Andrews, G. T.; Colquhoun, I. J.; McFarlane, W.; Grim, S. O. *J. Chem. Soc., Dalton Trans.* **1982**, 2353-2358.
16. Recent reviews: (a) Herrmann, W. A. *Angew. Chem., Int. Ed.* **2002**, *41*, 1290-1309. (b) Jafarpour, L.; Nolan, S. P. *Adv. Organomet. Chem.* **2001**, *46*, 181-222. (c) Herrmann, W. A.; Weskamp, T.; Böhm, V. P. *Adv. Organomet. Chem.* **2001**, *48*, 1-69. (d) Herrmann, W. A.; Köcher, C. *Angew. Chem., Int. Ed.* **1998**, *36*, 2163-2187.
17. Representative examples: (a) Jackstell, R.; Andreau, M. G.; Frisch, A.; Selvakumar, K.; Zapf, A.; Klein, H.; Spannenberg, A.; Röttger, D.; Briel, O.; Karch, R.; Beller, M. *Angew. Chem., Int. Ed.* **2002**, *41*, 986-989. (b) Tan, K. L.; Bergman, R. G.; Ellman, J. A. *J. Am. Chem. Soc.* **2002**, *124*, 3202-3203. (c) Albrecht, M.; Crabtree, R. H.; Mata, J.; Peris, E. *Chem. Commun.* **2002**, 32-33. (d) Batey, R. A.; Shen, M.; Lough, A. J. *Org. Lett.* **2002**, *4*, 1411-1414. (e) Peris, E.; Loch, J. A.; Mata, J.; Crabtree, R. H. *Chem. Commun.* **2001**, 201-202. (f) Mathews, C. J.; Smith, P. J.; Welton, T.; White, A. J. P.; Williams, D. J. *Organometallics* **2001**, *20*, 3848-3850 (g) Powell, M. T.; Hou, D.-R.; Perry, M. C.; Cui, X.; Burgess, K. *J. Am. Chem. Soc.* **2001**, *123*, 8878-8879. (h) Tulloch, A. D.; Danopoulos, A. A.; Tooze, R. P.; Cafferkey, S. M.; Kleinhenz, S.; Hursthouse, M. B. *Chem. Commun.* **2000**, 1247-1248. (i) McGuinness, D. S.; Cavell, K. J. *Organometallics* **2000**, *19*, 741-748. (j) Chen, J. C. C.;

Background

The σ-donor/π-acceptor synergism is an important theme in inorganic chemistry and applies to a wide variety of bonding situations. This concept of a synergism developed from the Dewar-Chatt-Duncanson model of metal–olefin bonding, which we understand to involve simultaneous donor (from the filled olefin π orbital to a metal-based orbital) and acceptor (from a filled metal orbital to the olefin π* orbital) components.[18] As taught to inorganic chemistry students worldwide, a similar model can be applied to the metal–carbonyl interaction, which is usually characterized by a combination of σ donation from the carbonyl lone pair to a metal-based orbital and π backbonding from a filled metal d orbital to the carbonyl π* orbital.[18] The σ-donor/π-acceptor model can be extended further to include phosphine and carbene ligands, as illustrated in Figure 5.2. Metal–phosphine bonding can be described by σ donation from the

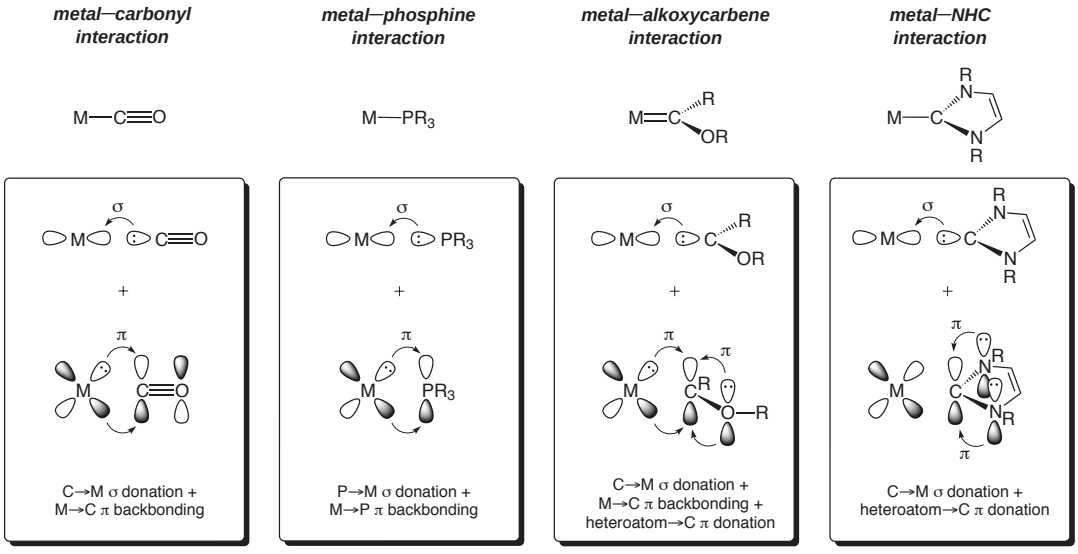

Figure 5.2

Lin, I. J. B. *Organometallics* **2000**, *19*, 5113-5121. (k) Gardiner, M. G.; Herrmann, W. A.; Reisinger, C.-P.; Schwarz, J.; Spiegler, M. *J. Organomet. Chem.* **1999**, *572*, 239-247. (l) Weskamp, T.; Böhm, V. P. W.; Herrmann, W. A. *J. Organomet. Chem.* **1999**, *585*, 348-352. (m) McGuinness, D. S.; Green, M. J.; Cavell, K. J.; Skelton, B. W.; White, A. H. *J. Organomet. Chem.* **1998**, *565*, 165-178. (n) Lappert, M. F.; Maskell, R. K. *J. Organomet. Chem.* **1984**, *264*, 217-228.

18. (a) Crabtree, R. H. *The Organometallic Chemistry of the Transition Metals*, 3rd Ed.; John Wiley & Sons: New York, 2001. (b) Elschenbroich, C.; Salzer, A. *Organometallics: A Concise Introduction*, 2nd Ed.; VCH: Weinheim, 1992. (c) Cotton, F. A.; Wilkinson, G. *Advanced Inorganic Chemistry*, 5th Ed.; John Wiley & Sons: New York, 1988. (d) Collman, J. P.; Hegedus, L. S.; Norton, J. R.; Finke, R. G. *Principles and Applications of Organotransition Metal Chemistry*; University Science Books: Mill Valley, CA, 1987.

phosphorus lone pair to the metal center and π backbonding from a filled metal orbital to the σ* P–R orbitals.[19] Likewise, in traditional "Fischer-type" metal carbenes, the σ-donor interaction involves the carbene lone pair and a metal-based orbital, and the π-backbonding interaction involves a filled metal orbital and the carbene p orbital. The bonding of NHC ligands can be viewed as an extreme Fischer-type case in which σ donation dominates the metal–carbene interaction.

The validity of the σ-donor/π-acceptor description of metal–olefin and –carbonyl interactions is supported by extensive experimental evidence, but it is not as well established for the metal–phosphine and –carbene interactions. The main points of continuing controversy are (1) the relative σ-donor strength of certain derivatives and (2) the extent of metal→ligand π backbonding.[20,21] The σ-donor strength refers to the ability of the lone pair to donate to a metal center; likewise, the π backbonding strength refers to the ability of the ligand to compete for electron density on the metal.

I. $(CO)_5Mo(L)$ Complexes

In this study, we address the question of whether the NHC ligand can act in a π-acceptor capacity in addition to being a σ-donor ligand. From previous work, it is clear that π backbonding is not a prerequisite for metal–NHC bonding; for example, NHCs can coordinate to atoms largely incapable of π backbonding, such as lanthanides and alkali metals.[22] However, we want to know if π backbonding is *possible* under the appropriate conditions, which would have important ramifications in catalysis.

We seek to separate and quantify the ligand→metal (σ donor) and metal→ligand (π acceptor) components of the bonding in a series $(CO)_5Mo(L)$ molecules. This information is important from both theoretical and practical points of view. Importantly, the σ-donor and π-acceptor components do not contribute equally to the overall bonding interaction, and thus they do not influence reactivity in the same way. In addition, we would like to test current bonding

---

19. (a) Orpen, A. G.; Connelly, N. G. *Organometallics* **1990**, *9*, 1206-1210. (b) Orpen, A. G.; Connelly, N. G. *J. Chem. Soc., Chem. Commun*. **1985**, 1310-1311. (c) Xiao, S.-X.; Trogler, W. C.; Ellis, D. E.; Berkovitch-Yellin, Z. *J. Am. Chem. Soc*. **1983**, *105*, 7033-7037.
20. Wang, S. P.; Richmond, M. G.; Schwartz, M. *J. Am. Chem. Soc*. **1992**, *114*, 7595-7596.
21. Magmusson, E. *Aust. J. Chem*. **1985**, *38*, 23-46.
22. Schumann, H.; Glanz, M.; Winterfeld, J.; Hemling, H.; Kuhn, N.; Kratz, T. *Angew. Chem., Int. Ed. Engl*. **1994**, *33*, 1733-1734.

models and further refine our understanding of metal–ligand bonding so that it becomes a better predictive too for organometallic reactivity.

Results and Discussion

Synthesis and structures of $(CO)_5Mo(L)$. For this study, we selected a range of L ligands that included several tertiary phosphines, trimethylamine as a representative tertiary amine, and 1,3-diisopropyl-4,5-dimethylimidazol-2-ylidene ($Pr^i_2Me_2Im$) as a representative NHC. We chose this particular NHC because it is one of the more widely used derivatives,[23,24] and because its small size aids the sublimation of $(CO)_5Mo(L)$ molecules for gas-phase photoelectron spectroscopy.[25]

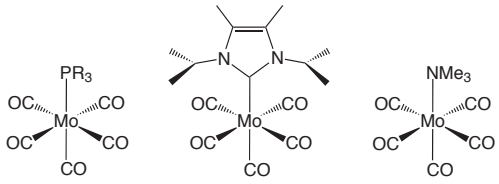

A variety of $(CO)_5Mo(L)$ complexes were prepared by standard methods. For example, $(CO)_5Mo(NMe_3)$ was synthesized by the reaction of molybdenum hexacarbonyl with trimethylamine and trimethylamine *N*-oxide.[26] The addition of PCy_3 to $(CO)_5Mo(NMe_3)$ displaces the labile NMe_3 ligand and cleanly provides $(CO)_5Mo(PCy_3)$. $(CO)_5Mo(Pr^i_2Me_2Im)$ was obtained by direct reaction of the free $Pr^i_2Me_2Im$ ligand with molybdenum hexacarbonyl. $(CO)_5Mo(H_2IMes)$ and $(CO)_5Mo(Ph_3Tri)$ were prepared from $(CO)_6Mo$ and the respective NHC adducts, $H_2IMes(H)(OBu^t)$ and $Ph_3Tri(H)(OMe)$.

The crystal structures of several $(CO)_5Mo(L)$ complexes and the $Pr^i_2Me_2Im$ free carbene are shown in Figures 5.3-59. Selected bond lengths and angles for some of these molecules and

---

23. Synthesis of $Pr^i_2Me_2Im$: Kuhn, N.; Kratz, T. *Synthesis-Stuttgart* **1993**, 561-562.
24. (a) Schumann, H.; Gottfriedsen, J.; Glanz, M.; Dechert, S.; Demtschuk, J. *J. Organomet. Chem.* **2001**, *617-618*, 588-600. (b) Foerstner, J.; Kakoschke, A.; Goddard, R.; Rust, J.; Wartchow, R.; Butenschön, H. *J. Organomet. Chem.* **2001**, *617-618*, 412-422. (c) Burford, N.; Cameron, T. S.; LeBlanc, D. J.; Phillips, A. D.; Concolino, T. E.; Lam, K.-C.; Rheingold, A. L. *J. Am. Chem. Soc.* **2000**, *122*, 5413-5414. (d) Louie, J.; Grubbs, R. H. *Chem. Commun.* **2000**, 1479-1480. (e) Stabenow, F.; Saak, W.; Weidenbruch, M. *Chem. Commun.* **1999**, 1131-1132. (f) Kuhn, N.; Fahl, J.; Fawzi, R.; Maichle-Mößmer, C.; Steimann, M. *Z. Naturforsch.* **1998**, *53b*, 720-726. (g) Kuhn, N.; Fahl, J.; Boese, R.; Henkel, G. *Z. Naturforsch.* **1998**, *53b*, 881-886. (h) Danopoulos, A. A.; Hankin, D. M.; Wilkinson, G.; Cafferkey, S. M.; Sweet, T. K. N.; Hursthouse, M. B. *Polyhedron* **1997**, *16*, 3879-3892. (i) Black, S. J.; Hibbs, D. E.; Hursthouse, M. B.; Jones, C.; Abdul Malik, K. M.; Smithies, N. A. *J. Chem. Soc., Dalton Trans.* **1997**, 4313-4319. (j) Kuhn, N.; Kratz, T.; Bläser, D.; Boese, R. *Chem. Ber.* **1995**, *128*, 245-250. (k) Kuhn, N.; Kratz, T.; Bläser, D.; Boese, R. *Inorg. Chim. Acta* **1995**, *238*, 179-181.
25. We have found that $(CO)_5Mo(L)$ complexes coordinated with larger NHCs, such as H_2IMes, do not sublime under PES conditions. Decomposition of these complexes occurs at elevated temperatures.
26. Maher, J. M.; Beatty, R. P.; Cooper, N. J. *Organometallics* **1985**, *4*, 1354-1361.

related $(CO)_5Mo(L)$ derivatives are collected in Tables 5.1 and 5.2. For comparison, the structure of molybdenum hexacarbonyl was redetermined at low temperature.[27] The structure of $(CO)_5Mo(PCy_3)$ also was determined recently by Valente and coworkers.[28]

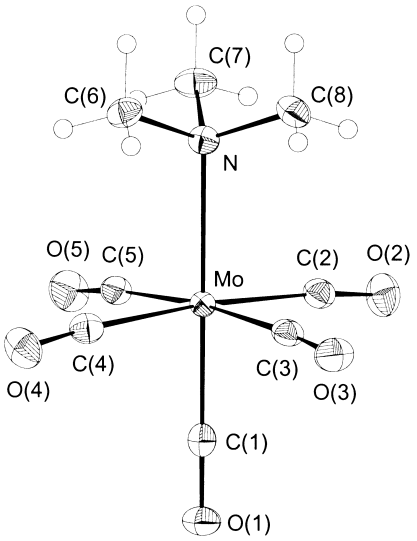

Figure 5.3: Structure of $(CO)_5Mo(NMe_3)$ (CCDC # 183991). Displacement ellipsoids are drawn at 50% probability; hydrogens atoms are drawn at arbitrary scale.

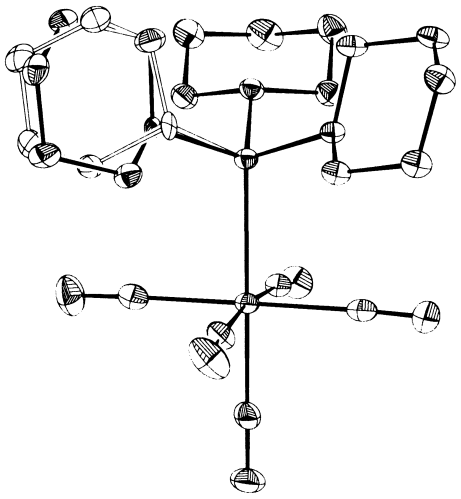

Figure 5.4: Structure of $(CO)_5Mo(PCy_3)$ (CCDC #176873). For clarity, all hydrogen atoms have been omitted. Displacement ellipsoids are drawn at 50% probability. The outlined set of ellipsoids indicates a disordered cyclohexyl ring.

27. CCDC # 191387. Original structure determination: Mak, T. C. W. *Z. Kristallogr*. **1984**, *166*, 277-281.
28. Cortes-Figueroa, J. E.; Leon-Velazquez, M. S.; Ramos, J.; Jasinski, J. P.; Deene, D. A.; Zubkowski, J. D.; Valente, E. J. *Acta Cryst*. **2000**, *C56*, 1435-1437

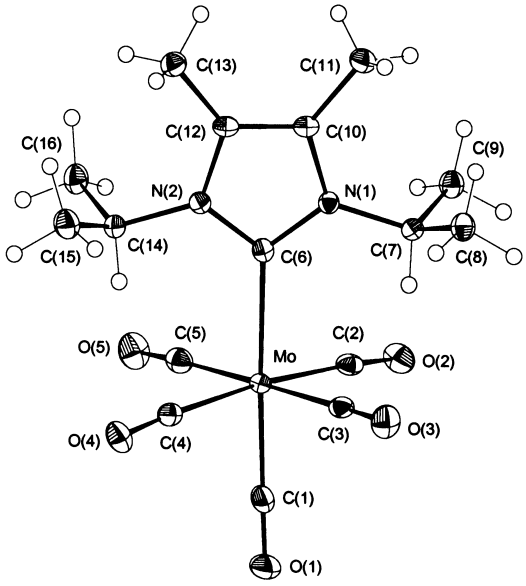

Figure 5.5: Structure of $(CO)_5Mo(Pr^i_2Me_2Im)$ (CCDC #157341). Displacement ellipsoids are drawn at 50% probability; hydrogen atoms are drawn at arbitrary scale.

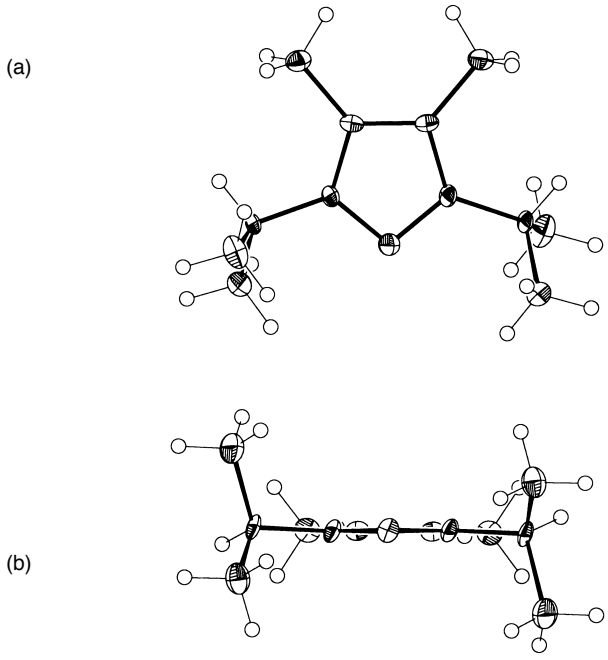

Figure 5.6: Structure of the $Pr^i_2Me_2Im$ free carbene with both top (a) and side (b) views (CCDC #192767).

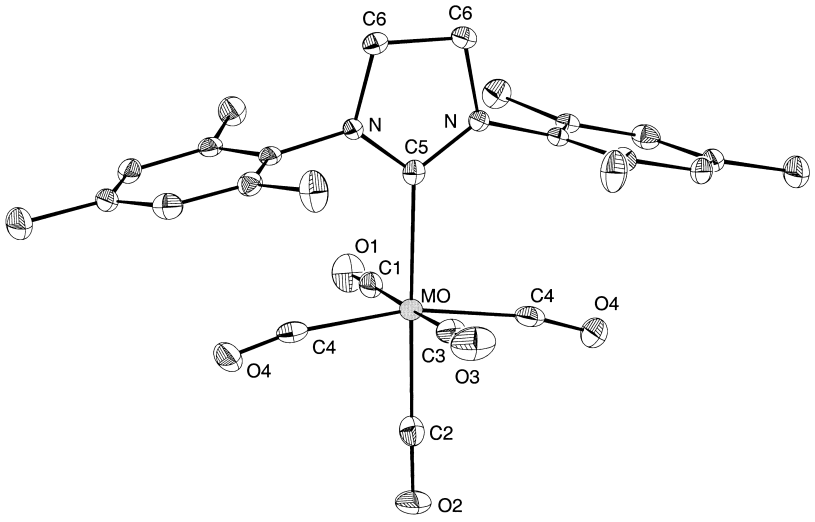

Figure 5.7: Structure of $(CO)_5Mo(H_2IMes)$ (CCDC #183571). Displacement ellipsoids are drawn at 50% probability; hydrogens atoms are drawn at arbitrary scale.

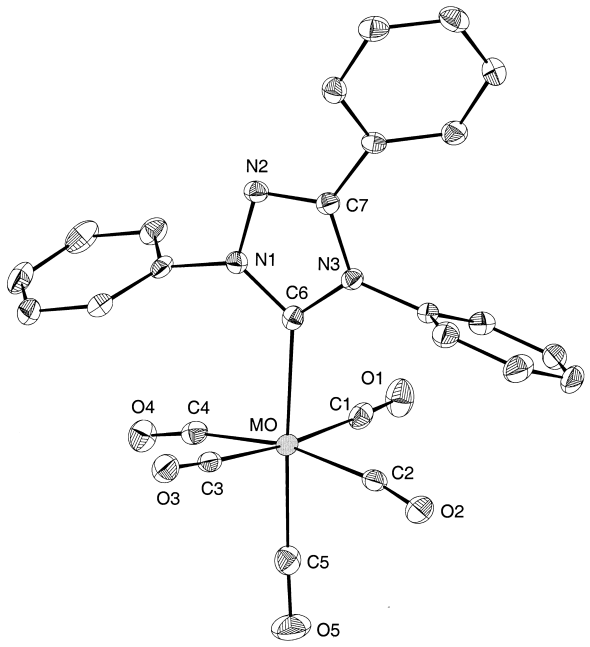

Figure 5.8: Structure of $(CO)_5Mo(Ph_3Tri)$ (CCDC #150145). Displacement ellipsoids are drawn at 50% probability; hydrogens atoms are drawn at arbitrary scale.

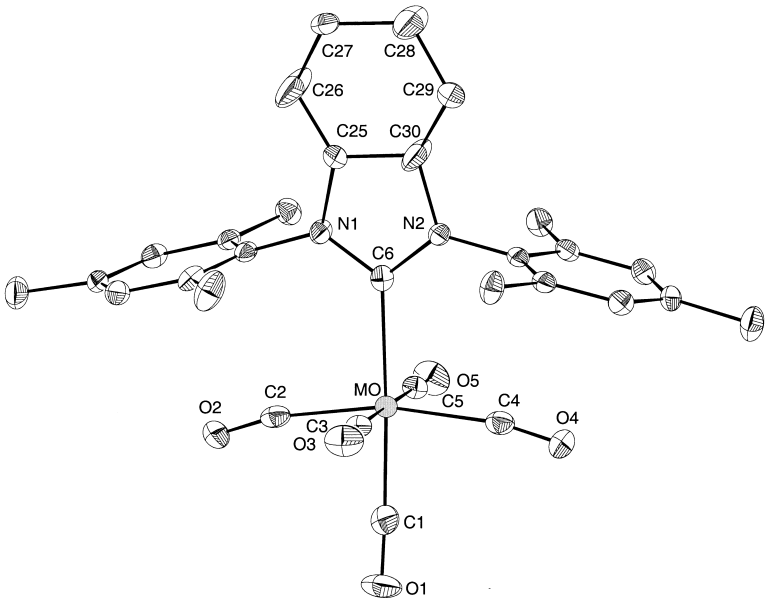

Figure 5.9: Structure of $(CO)_5Mo(CyMesIm)$ (CCDC #157420). Displacement ellipsoids are drawn at 50% probability; hydrogens atoms are drawn at arbitrary scale.

Table 5.1: Comparison of $(CO)_5Mo(L)$ bond distances (Å), angles (deg), and L cone angles (deg).

L	Ref.	Mo–L	Mo–C_{ax}	C▪O_{ax}	Mo–C_{eq} (avg)	C▪O_{eq} (avg)	Mo–C▪O_{ax}	Mo–C▪O_{eq} (avg)	L cone angle (xtal;[g] theo[h])	
CO	[a]	—	2.059(3)	1.125(5)	2.059(3)	1.125(5)	179.3(4)	179.3(4)	—	—
	[j]	—	2.059(1)	1.137(1)	2.059(1)	1.137(1)	179.5(1)	179.5(1)		
PF_3	[b]	2.37(1)	2.06(1)	1.15(1)	2.06(1)	1.15(1)	—	175(2)	—	104(2)
PCl_3	[c]	2.379(1)	2.035(2)	1.137(3)	2.052(2)	1.131(2)	179.4(2)	178.3(2)	—	124(2)
PPh_3	[e]	2.560(1)	1.995(3)	1.142(4)	2.046(4)	1.134(4)	178.3(3)	177.2(3)	148(5)	145(2)
$Pr^i_2Me_2Im$	[j]	2.311(2)	1.991(2)	1.152(2)	2.047(2)	1.142(2)	178.4(2)	176.9(2)	—	—
PMe_3	[d]	2.508(1)	1.984(3)	1.152(3)	2.036(5)	1.134(3)	179.7(4)	179.3(4)	111(2)	118(2)
PCy_3	[f]	2.594(2)	1.972(6)	1.154(6)	2.028(7)	1.148(6)	177.7(2)	175.6(2)	160(5)	170(2)
	[j]	2.583(1)	1.989(2)	1.147(2)	2.044(2)	1.140(2)	179.8(2)	176.0(2)		
NMe_3	[j]	2.369(1)	1.955(1)	1.158(2)	2.051(1)	1.137(2)	179.5(1)	174.8(1)	—	132(2)[f]

[a] Mak, T. C. W. *Z. Kristallogr.* **1984**, *166*, 277-281; [b] (gas-phase electron diffraction) Bridges, D. M.; Holywell, G. C.; Rankin, D. W. H.; Freeman, J. M. *J. Organomet. Chem.* **1971**, *32*, 87-95; [c] Frenking, G.; Wichmann, K.; Fröhlich, N.; Grobe, J.; Golla, W.; Le Van, D.; Krebs, B.; Läge, M. *Organometallics* **2002**, *21*, 2921-2930; [d] Davies, M. S.; Aroney, M. J.; Buys, I. E.; Hambley, T. W.; Calvert, J. L. *Inorg. Chem.* **1995**, *34*, 330-336; [e] Cotton, F. A.; Darensbourg, D. J.; Ilsley,

W. H. *Inorg. Chem.* **1981**, *20*, 578-583; [f] Cortes-Figueroa, J. E.; Leon-Velazquez, M. S.; Ramos, J.; Jasinski, J. P.; Deene, D. A.; Zubkowski, J. D.; Valente, E. J. *Acta Cryst.* **2000**, *C56*, 1435-1437; [g] averaged crystallographic cone angles for all complexes in the Cambridge Structural Database; Müller, T. E.; Mingos, D. M. P. *Trans. Met. Chem.* **1995**, *20*, 533-539; [h] idealized/theoretical (Tolman) cone angles; Tolman, C. A. *Chem. Rev.* **1977**, *77*, 313-348; [i] Seligson, A. L.; Trogler, W. C. *J. Am. Chem. Soc.* **1991**, *113*, 2520-2527; [j] this work.

Table 5.2: Comparison of selected $(CO)_5Mo(L)$ bond distances (Å) and angles (deg) with those in the corresponding free ligands.

Complex	Free L	Ref. For free L	Average distances (bond; in complex; in free L)			Average angles (angle; in complex; in free L)		
$(CO)_5Mo(NMe_3)$	NMe_3	[a]	N–C	1.484(2)	1.451(3)	C–N–C	107.5(1)	110.9(6)
$(CO)_5Mo(PF_3)$	PF_3	[b]	P–F	1.557(4)	1.570(1)	F–P–F	99.5(5)	97.8(2)
$(CO)_5Mo(PCl_3)$	PCl_3	[c]	P–Cl	2.031(1)	2.043(3)	Cl–P–Cl	99.9(1)	100.1(3)
$(CO)_5Mo(PMe_3)$	PMe_3	[d]	P–C	1.811(3)	1.846(3)	C–P–C	102.7(4)	98.6(3)
$(CO)_5Mo(PPh_3)$	PPh_3	[e]	P–C	1.834(3)	1.831(2)	C–P–C	115.6(1)	102.8(1)
$(CO)_5Mo(PCy_3)$	PCy_3	[f]	P–C	1.865(2)	1.868(6)	C–P–C	105.9(2)	103.8(3)
$(CO)_5Mo(Pr^i{}_2Me_2Im)$	$Pr^i{}_2Me_2Im$	[g]	C–N	1.367(2)	1.364(1)	N–C–N	103.6(2)	101.9(1)

[a] (structure by rotational spectroscopy) Wollrab, J. E.; Laurie, V. W. *J. Chem. Phys.* **1969**, *51*, 1580-1583; [b] (gas-phase electron diffraction) Morino, Y.; Kuchitsu, K.; Moritani, T. *Inorg. Chem.* **1969**, *8*, 867-871; [c] (structure by gas-phase microwave spectroscopy) Kisliuk, P.; Townes, C. H. *J. Chem. Phys.* **1950**, *18*, 1109-1111; [d] (structure by gas-phase electron diffraction) Bartell, L. S.; Brockway, L. O. *J. Chem. Phys.* **1960**, *32*, 512-515; [e] Dunne, B. J.; Orpen, A. G. *Acta Cryst.* **1991**, *C47*, 345-347; [f] Davies, J. A.; Dutremez, S.; Pinkerton, A. A. *Inorg. Chem.* **1991**, *30*, 2380-2387; [g] this work.

The Mo–L bond distances vary, but there are many factors that influence this parameter: the bonded atom, the steric parameters of the ligand, and the electronics of the ligand. This makes any constructive comment difficult. However, the steric impact on the axial carbonyl should be minimal, so metrical changes of this ligand may have some electronic significance. In all $(CO)_5Mo(L)$ structures, the structural trans influence of the L ligands causes the axial carbonyl ligand to contract along the Mo–C bond and elongate along the C≡O bond because of increased Mo→CO π backbonding. Compared to $(CO)_6Mo$, the maximum $Mo–C_{ax}$ contraction of 0.104 Å occurs in $(CO)_5Mo(NMe_3)$. The maximum $C{\equiv}O_{ax}$ elongation of 0.021 Å occurs in

$(CO)_5Mo(NMe_3)$ as well. The maximum Mo–C_{eq} contraction is of much smaller magnitude, of up to 0.023 Å in $(CO)_5Mo(PMe_3)$, and any C≡O_{eq} elongation is non-existent.

All Mo–C≡O_{ax} angles are essentially linear. On average, the Mo–C≡O_{eq} angles are slightly bent away from L (up to 4.4°) when the ligand is bulky, as in PCy_3 and $Pr^i_2Me_2Im$, but curiously, they are bent even further when L is NMe_3 (by 5.2°).

There are significant differences in the structures of $(CO)_6Mo$ and $(CO)_5Mo(PCy_3)$ determined at lower (98 K) and higher (293-295 K) temperatures. For $(CO)_6Mo$, we see lengthening of the C≡O bond at lower temperature by 0.012 Å. For $(CO)_5Mo(PCy_3)$, we see the largest differences in the Mo–P distance (a decrease of 0.011 Å at lower temperature), the Mo–C_{ax} distance (an increase of 0.017 Å at lower temperature), the Mo–C_{eq} distance (an increase of 0.016 Å at lower temperature), and the Mo–C≡O_{ax} angle (an increase of 2.1° at lower temperature). As always, due caution in comparing structural parameters is necessary.

In $(CO)_5Mo(Pr^i_2Me_2Im)$, a staggered tetracarbonyl arrangement is enforced by the isopropyl protons positioned between adjacent carbonyl ligands (Figure 5.5), in contrast to the arrangement in $(CO)_5Mo(H_2IMes)$ (Figure 5.7). However, the isopropyl groups in the free ligand $Pr^i_2Me_2Im$ are oriented in the opposite direction and adopt a slightly staggered arrangement.[29] This arrangement helps protect the carbene lone pair and improve the stability of the free NHC.

Table 5.2 describes changes in geometry upon ligand binding. For L = PPh_3, PCy_3, and $Pr^i_2Me_2Im$, the X–Y bonds (P–C or C–N) in the coordinated ligand and the free ligand are identical within error (using 3σ as a realistic error estimate). However, the Y–X–Y angles (C–P–C or N–C–N) are consistently smaller in the free ligand compared to the bound ligand, by up to 12.8(1)° for L = PPh_3. For L = NMe_3, PF_3, PCl_3, and PMe_3, there are also variations between the bond lengths and angles in the complex and free ligand, but because the structures of the free ligands were obtained in the gas phase by a variety of techniques, it is difficult to make comparisons. In general, we can conclude that there is no obvious correlation between the properties of L and structural changes in $(CO)_5Mo(L)$ complexes.

Photoelectron spectroscopy.[30] This crystal structure information provides valuable information about the three-dimensional ground-state structures of $(CO)_5Mo(L)$ complexes and the steric environment of the L ligands. However, the electronic structure of these molecules is a critical aspect of their reactivity. A direct method to study electronic structure is photoelectron

29. Alder and co-workers have predicted that the isopropyl groups adopt an eclipsed arranged in the preferred conformation. Alder, R. W.; Allen, P. R.; Williams, S. J. *Chem. Commun.* **1995**, 1267-1268.

spectroscopy, which provides a measure of the ionization potentials of a molecule. These ionization energies are directly related to the energy levels of distinct molecular orbitals.

As illustrated in Figure 5.10, a $(CO)_6Mo$ molecule in octahedral symmetry has a triply degenerate t_{2g} set of orbitals. When one carbonyl ligand is placed with another ligand L, the symmetry descends to C_{4v}, which causes the t_{2g} orbitals to split into b_2 and e sets.

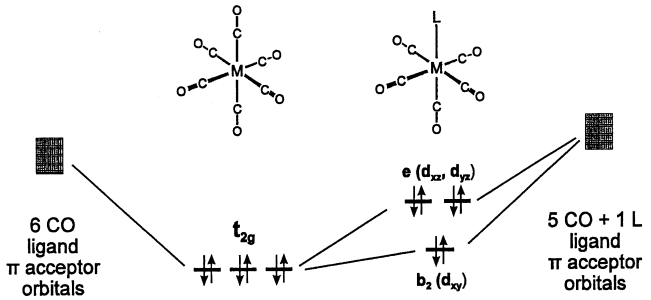

Figure 5.10

Figure 5.11 shows the close-up metal ionization regions of the photoelectron spectra for $(CO)_6Mo$ and a series of $(CO)_5Mo(L)$ molecules, where L = trimethylphosphine (PMe_3), triphenylphosphine (PPh_3), tricyclohexylphosphine (PCy_3), and the N-heterocyclic carbene $Pr^i_2Me_2Im$. The 2:1 ratio band structure is consistent for all $(CO)_5Mo(L)$ molecules and reflects the degeneracies of the e and b_2 sets. The first ionization feature (at lowest ionization energy) is assigned as the metal e orbital set and designated M1/M2, whereas the b_2 ionization is designated as M3. In all experiments, instrument resolution was high enough to observe a shoulder off of the M3 ionization, which is assigned as the vibrational stretching frequency of carbonyl (ν_{CO}) and designated M3′.

Data for $(CO)_6Mo$ has been reported previously,[31] but it was re-collected under high-resolution conditions for this study. The ionizations from the triply degenerate molybdenum t_{2g} orbitals occur at 8.38 eV (Figure 5.11 **A**).

---

30. These studies were done in collaboration with Prof. Dennis Lichtenberger and Tonja Bill at the University of Arizona.
31. (a) Cooper, G., Green, J.C., Payne, M. P., Dobson, B. R., Hillier, I. H. *J. Am. Chem. Soc.* **1987**, *109*, 3836-43. (b) Hubbard, J. L., Lichtenberger, D. L. *J. Am. Chem. Soc.* **1982,** *104*, 2132-8.

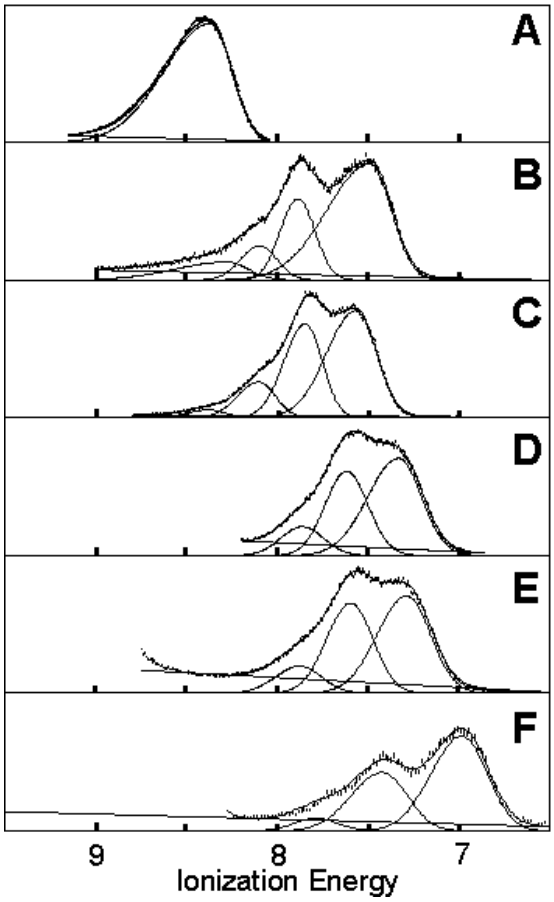

Figure 5.11: He I photoelectron spectra for the metal ionizations for $(CO)_5Mo(L)$; L = CO (**A**), NMe_3 (**B**), PMe_3 (**C**), PPh_3 (**D**), PCy_3 (**E**) and $Pr^i_2Me_2Im$ (**F**).

The photoelectron spectrum for $(CO)_5Mo(NMe_3)$ (Figure 5.11 **B**) displays the same 2:1 ration of the e to b_2 orbitals, which is consistent with the symmetry of these molecules. The ionizations from the e orbital for this amine complex occur at 7.49 eV, and the b_2 at 7.88 eV, with the vibrational stretching of the CO resolved at 8.09 eV.

The spectrum for $(CO)_5Mo(PMe_3)$ (Figure 5.11 **C**), which has been previously reported,[32] shows ionizations from the e orbital (M1/M2) at 7.57 eV and from the b_2 orbital (M3) at 7.85 eV. Two vibrational progressions for the carbonyl stretching frequencies (ν_{CO}) were resolved at 8.10

32. (a) Puddenphatt, R. J., Dignardbailey, L., Bancroft, G. M. *Inor. Chim. Acta – Articles and Letters* **1985**, *96*, L91. (b) Ikuta, S., Kebarle, P., Bancroft, G. M., Chan, T., Puddenphatt, R. J. *J. Am. Chem. Soc.* **1982**, *104*, 5899. (c) Lichtenberger, D. L., Jatcko, M. E. *Inorg. Chem.* **1992**, *31*, 451.

eV and 8.37 eV. Ionizations for the metal orbitals of triphenylphosphine (Figure 5.11 **D**) occur at 7.33 eV for the e (M1/M2) and 7.62 eV for the b_2, with the stretching frequency of CO at 7.86 eV. Of the series of molybdenum pentacarbonyl phosphine complexes, $(CO)_5Mo(PCy_3)$ has the lowest ionization energy for the e orbitals at 7.29 eV, with the b_2 at 7.60 eV and ν_{CO} at 8.87 eV (Figure 5.11 **E**).

The photoelectron spectrum for $(CO)_5Mo\ Pr^i_2Me_2Im$ in Figure 5.11 **F** shows the same basic features as for the phosphine analogs. Metal based ionizations correlating to the M1/M2 ionizations are seen at 6.98 eV, and the M3 and M3′ ionizations are at 7.42 eV and 7.70 eV, respectively.

Photoelectron spectroscopy provides the most conclusive results regarding the σ donor and π acceptor ability of ligands. With this experiment, we have been able to successfully separate and quantify the σ and π components in a series of molybdenum-phosphine, -amine, and -NHC bonds. As shown in previous photoelectron investigations of metal-phosphine complexes, the outer valence electronic structure leads to ionizations that correlate to the metal d orbitals. Focusing on the metal-based ionizations in Figure 5.11 **B**-**F**, it is recognized that the metal orbitals is split into the e and b_2 symmetry sets under the C_{4v} symmetry of the $(CO)_5Mo(L)$ molecule (Figure 5.10). The two orbitals that form the e set each backbond to three CO ligands and L. The remaining b_2 orbital backbonds to the four carbonyls in the equatorial plane that are cis to L. The primary difference between the stabilization of the b_2 orbital and the e is the variance in backbonding ability between the carbonyl ligands, and the phosphine or carbene ligand. Because CO is such a strong π-backbonding ligand, the b_2 ionization with its four interactions with carbonyl is stabilized to higher ionization energy compared to the two orbitals comprising the e set. For the complexes in this study, the energy separation between the e and b_2 is ~0.29 eV for $(CO)_5Mo(L)$ where L is a phosphine ligand. The consistency of the energy separation between the e and b_2 for the phosphine complexes indicates that the π stabilization is the same by this technique for each phosphine ligand studied.

To completely understand the π-acceptor ability of a ligand, the e-b_2 splitting for both strong π-acceptors and weak π-acceptors are compared. The strong π-acceptor CO ligand shows complete degeneracy of the t_{2g} orbitals and thus no splitting. On the other hand, a benchmark for the absence of π interactions is the $(CO)_5Mn(H)$ molecule in which the hydride ligand has no possibility of π-type interactions, and the observed e-b_2 splitting is 0.40 ± 0.02 eV in this

instance.[33] Comparison of this value to the splitting seen for the phosphine derivatives indicates that the phosphine ligands are weak π acceptors, and are approximately 25% as effective as the carbonyl ligand at π-backbonding.

In comparing the photoelectron spectrum of $(CO)_5Mo(Pr^i_2Me_2Im)$ to the spectra of the $(CO)_5Mo(PR_3)$ complexes, it is readily apparent that the electronic factors of the carbene complex differ substantially from the phosphines. First, the metal ionizations in the carbene molecule are destabilized compared to the phosphine systems. This is indicative of the greater electron richness at the metal center, a direct result of a large amount of electron density being donated from the carbene ligand to the metal. Second, the observed e-b_2 splitting is also greater than in the phosphine derivatives (0.44 eV). This value is in the range expected for ligands with no π-acceptor ability. Similarly, the e-b_2 splitting of $(CO)_5Mo(NMe_3)$ is also ~0.4 eV, which is consistent with the inability of this tertiary amine to participate in π backbonding.

The relative σ-donor abilities of these phosphine, amine, and NHC ligands is reflected by the first ionizations that correspond to the e set. The energy of these orbitals change in response to the electron density at the metal center. Using this measure, the σ-donor ability of L in $(CO)_5Mo(L)$ complexes increases in the order $PMe_3 < NMe_3 < PPh_3 < PCy_3 < Pr^i_2Me_2Im$.

These results are summarized in a plot of e ionization energy (σ-donor contribution) *versus* e-b_2 splitting (π-backbonding contribution) (Figure 5.12). This plot includes data points for L = PF_3, $P(OMe)_3$, $P(OEt)_3$, $P(NMe_2)_3$, PEt_3, and PBu^n_3 from the literature.[12] The error bars for L = PF_3, $P(OMe)_3$, $P(OEt)_3$, $P(NMe_2)_3$ are larger because of the lower resolution of those spectra. Overall, the σ-donor ability of L increases in the order $PF_3 << P(OMe)_3 < P(OEt)_3 < P(NMe_2)_3 < PMe_3 < PEt_3 < NMe_3 < PBu^n_3 < PPh_3 < PCy_3 << Pr^i_2Me_2Im$. This ordering is similar to that based on pK_a values and usually presented in textbooks, with the exception of PPh_3; triarylphosphines have lower pK_a values than trialkylphosphines, is interpreted as triarylphosphines being weaker σ donors.[34,35,36] However, gas-phase proton affinity data is consistent with the ordering found in this study, *i.e.*, the proton affinity of triarylphosphines is higher than that of trialkylphosphines. This difference is thought to be due to the effects of solvation in solution phase pK_a measurements. In comparison, the gas-phase information should provide more accurate data for comparison

33. Lichtenberger, D. L.; Sarapu, A. C.; Fenske, R. F. *Inorg. Chem.* **1973**, *12*, 702-705.
34. Suresh, C. H.; Koga, N. *Inorg. Chem.* **2002**, 41, 1573-1578.
35. Perrin, L.; Clot, E.; Eisenstein, O.; Loch, J.; Crabtree, R. H. *Inorg. Chem.* **2001**, *40*, 5806-5811.
36. Pacchioni, G.; Bagus, P. S. *Inorg. Chem.* **1992**, *31*, 4391-4398.

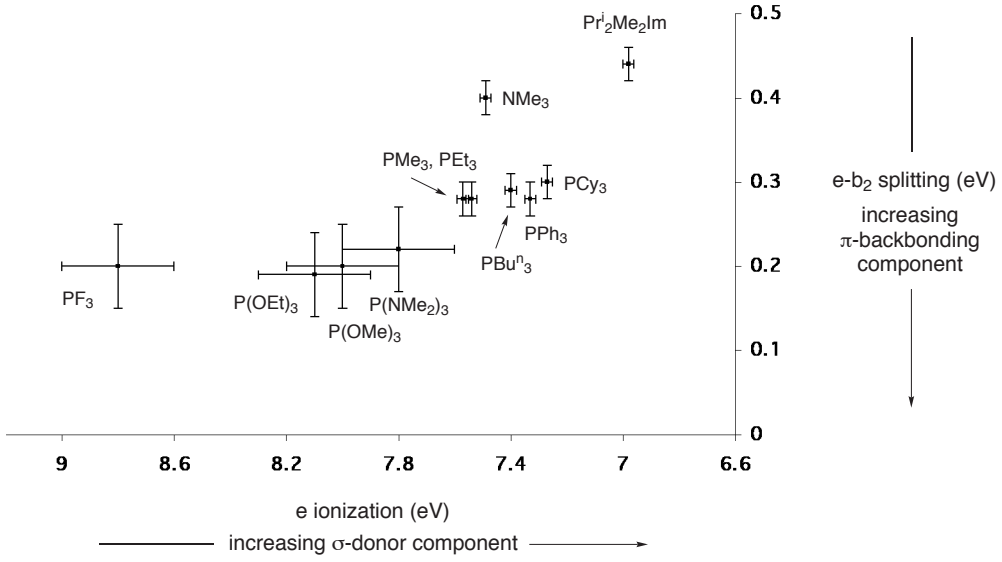

Figure 5.12

with calculations, and also more accurately reflect the bonding within a metal complex.

The π-backbonding ability of L increases in the order [Pr$^i_2$Me$_2$Im = NMe$_3$] < [PCy$_3$ = PPh$_3$ = PBu$^n_3$ = PEt$_3$ = PMe$_3$] < [PF$_3$ = P(OMe)$_3$ = P(OEt)$_3$ = P(NMe$_2$)$_3$]. As expected, PF$_3$, P(OMe)$_3$, P(OEt)$_3$, and P(NMe$_2$)$_3$ form the strongest π interactions. However, both the trialkyl- and triarylphosphine ligands appear to have weaker but comparable π interactions. This result contrasts with the generally accepted ordering that ranks trialkylphosphines as weaker π-backbonding ligands than triarylphosphines. The Quantitative Analysis of Ligand Effects (QALE) is consistent with the ordering obtained by PES in this study.[37] The PES results also reveal that neither the Pr$^i_2$Me$_2$Im ligand nor NMe$_3$ participate in π backbonding within the (CO)$_5$Mo(L) framework.

37. (a) Wilson, M. R.; Prock, A.; Giering, W. P.; Fernandez, A. L.; Haar, C. M.; Nolan, S. P.; Foxman, B. M. *Organometallics* **2002**, 21, 2758-2763. (b) Woska, D.; Prock, A.; Giering, W. P. *Organometallics* **2000**, 19, 4629-4638. (c) Fernandez, A.; Reyes, C.; Wilson, M. R.; Woska, D. C.; Prock, A.; Giering, W. P. *Organometallics* **1997**, *16*, 342-348. (d) Wilson, M. R.; Woska, D. C.; Prock, A.; Giering, W. P. *Organometallics* **1993**, *12*, 1742-1752. (e) Liu, H.-Y.; Eriks, K.; Prock, A.; Giering, W. P. *Organometallics* **1990**, *9*, 1758-1766. (f) Rahman, M. M.; Liu, H.-Y.; Eriks, K.; Prock, A.; Giering, W. P. *Organometallics* **1989**, *8*, 1-7. (g) Rahman, M. M.; Liu, H. Y.; Prock, A.; Giering, W. P. *Organometallics* **1987**, *6*, 650-658. (h) Golovin, M. N.; Rahman, M. M.; Belmonte, J. E.; Giering, W. P. *Organometallics* **1985**, *4*, 1981-1991.

Infrared and ^{95}Mo NMR spectroscopy. Traditionally, infrared spectroscopy has been used to extract information about bonding in organometallic complexes. The stretching frequencies for a series of $(CO)_5Mo(L)$ complexes are shown in Table 5.3. The fact that $(CO)_5Mo(Pr^i_2Me_2Im)$ has a low value compared to the other $(CO)_5Mo(L)$ derivatives is consistent with $Pr^i_2Me_2Im$ being a strong σ-donor ligand: this effect makes the metal center electron more rich, which in turn strengthens the trans Mo–CO interaction and weakens the C≡O interaction.

Table 5.3: IR data for $(CO)_6Mo(L)$ complexes (cm^{-1}), presented in order of decreasing ν_{CO} (A_1, CO_{ax}).

L	Ref.	Medium	ν_{CO} (A_1, CO_{ax})	additional ν_{CO}
PF_3	[a]	hexane	2101	2013, 1988
PCl_3	[b]	hexane	2095	2013, 2001, 1988
$P(OMe)_3$	[b]	hexane	2082	1997, 1970, 1956
PPh_3	[b]	hexane	2075	1989, 1950, 1945
NMe_3	[c]	hexane	2072	1941, 1921
	[f]	KBr pellet	2074	1927, 1916
PMe_3	[d]	cyclopentane	2071	1952, 1945
PCy_3	[e]	hexane	2066	1989, 1941, 1937
	[f]	KBr pellet	2064	1975, 1936, 1913
$Pr^i_2Me_2Im$	[f]	KBr pellet	2061	1973, 1922, 1911, 1888
CO	[b]	hexane	1989	—
	[f]	KBr pellet	1982	—

[a] Denham, E. L.; Clark, R. J. *J. Chromatography* **1984**, *301*, 253-260; [b] Darensbourg, D. J.; Brown, T. L. *Inorg. Chem.* **1968**, *7*, 959-966; [c] Koelle, U. *J. Organomet. Chem.* **1977**, *133*, 53-58; [d] Davies, M. S.; Pierens, R. K.; Aroney, M. J. *J. Organomet. Chem.* **1993**, *458*, 141-146; [e] Gao, Y.-C.; Shi, Q.-Z.; Kershner, D. L.; Basolo, F. *Inorg. Chem.* **1988**, *27*, 188-191; [f] this work.

However, such a relationship is not observed when L is varied among different NHC ligands, such as $Pr^i_2Me_2Im$, H_2IMes, IMes, Ph_3Tri, and so on.[38] The values for the A_1 band in these derivatives are scattered in the range of ~ 2075-2060 cm^{-1}, and no conclusions can be made about the relative σ-donor abilities of NHCs as the *N*-substituents or the backbone is modified.

38. Examples: (a) $(CO)_5Mo[C(NH)_2(CH_2)_3]$ (2063 cm^{-1}), reference 11c. (b) $(CO)_5Mo[C(NMe)_2(CH_2)_2]$ (2064 cm^{-1}), $(CO)_5Mo[C(NEt)_2(CH_2)_2]$ (2060 cm^{-1}) and $(CO)_5Mo[C(NCH_2Ph)_2(CH_2)_2]$ (2065 cm^{-1}) Lappert, M. F.; Pye, P. L.; McLaughlin, G. M. *J. Chem. Soc., Dalton Trans.* **1977**, 1272-1282.

A similar situation is presented by ^{95}Mo NMR chemical shifts, which have been used by Alyea and coworkers to estimate the relative σ-donor and π-acceptor contributions to Mo–L bonding in a series of $(CO)_5Mo(L)$ complexes, where L = phosphines and substituted pyridines.[15] It is difficult to compare ^{95}Mo NMR values for L = phosphine versus L = NHC because the very different steric effects of these ligands have a significant impact on chemical shift. In addition, the values for a series of isostructural NHCs (H_2IMes, IMes, and Cl_2IMes, in which the *N*-mesityl substituents remain constant but the ligand backbone is varied) shows no clear trend.

II. Cp*Ru(Cl)(L) and Cp*Ru(Cl)(CO)(L)

Unfortunately, $(CO)_5Mo(L)$ complexes where L = H_2IMes, IMes, Cl_2IMes, and other relatively large NHCs, were not amenable to PES analysis because they would not sublime. It is important to study these more subtle ligand effects because it is known that they can have a large impact on catalytic activity. For this reason, we began to examine Cp*Ru(Cl)(L) and Cp*Ru(Cl)(L)(CO) complexes, where L is a phosphine or N-heterocyclic carbene ligand.

Synthesis of Cp*Ru(Cl)(L) and Cp*Ru(Cl)(L)(CO) complexes. As illustrated in Scheme 5.1, a variety of Cp*Ru(Cl)(L) complexes were prepared by standard methods.[39] The

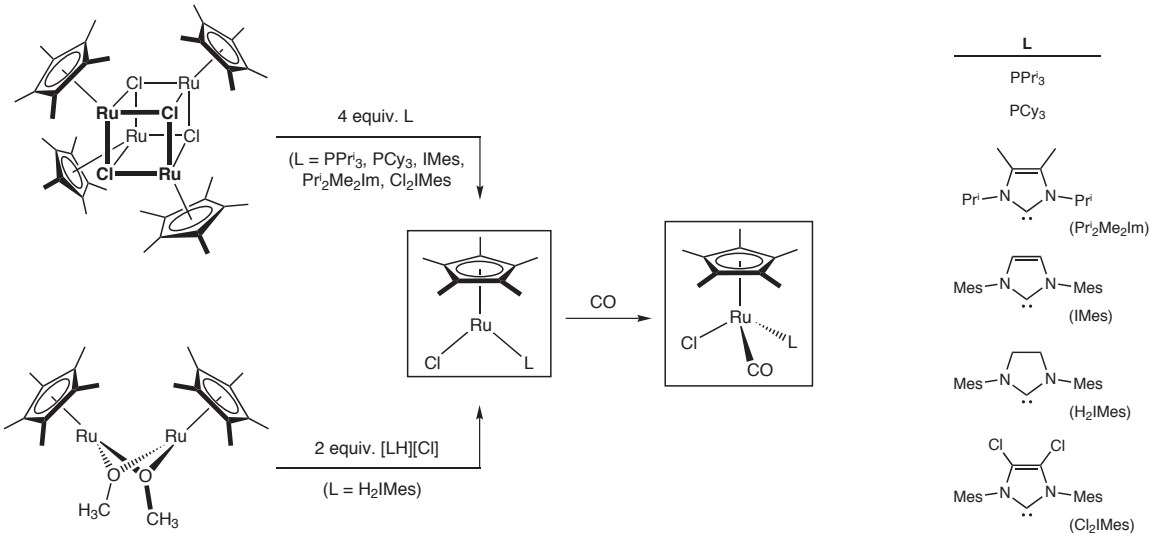

Scheme 5.1

39. [39] (a) Baratta, W.; Herrmann, W. A.; Rigo, P.; Schwarz, J. *J. Organomet. Chem.* **2000**, *593-594*, 489-493. (b) Campion, B. K.; Heyn, R. H.; Tilley, T. D. *J. Chem. Soc., Chem. Commun.* **1988**, 278-280.

derivatives where L = PPr^i_3, PCy_3, IMes, $Pr^i_2Me_2Im$, and Cl_2IMes were synthesized by the reaction of $[Cp^*RuCl]_4$ tetramer with the free NHC. Alternatively, $Cp^*Ru(Cl)(H_2IMes)$ could be synthesized more conveniently from the reaction of the $[Cp^*Ru(OMe)]_2$ dimer with the H_2IMes chloride salt. The carbonyl complexes were obtained by simply reaction the 16-electron $Cp^*Ru(Cl)(L)$ complexes with an excess of carbon monoxide gas. The crystal structures of several derivatives are shown in Figures 5.13-5.16.

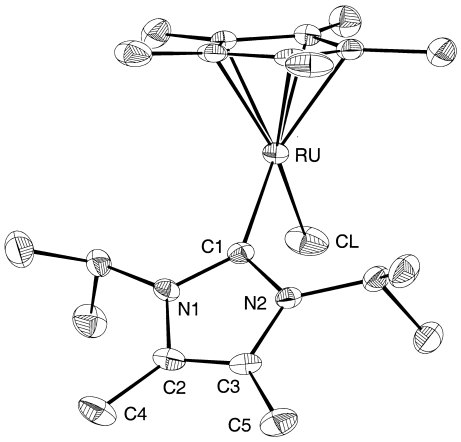

Figure 5.13: Structure of $Cp^*Ru(Cl)(Pr^i_2Me_2Im)$ (CCDC #176873). For clarity, all hydrogen atoms have been omitted. Displacement ellipsoids are drawn at 50% probability.

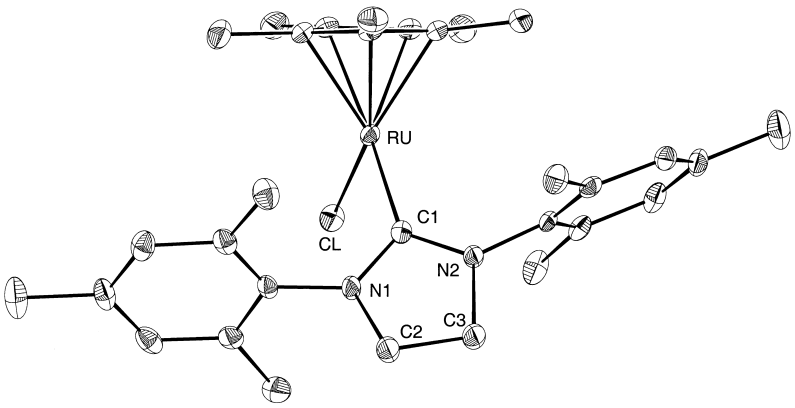

Figure 5.14: Structure of $Cp^*Ru(Cl)(H_2IMes)$ (CCDC #176873). For clarity, all hydrogen atoms have been omitted. Displacement ellipsoids are drawn at 50% probability.

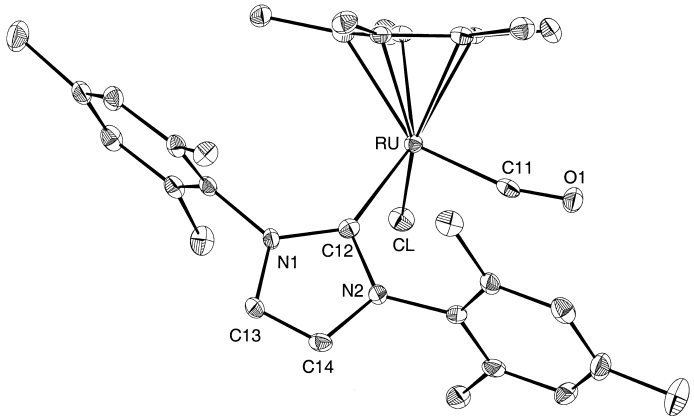

Figure 5.15: Structure of Cp*Ru(Cl)(CO)(IMes) (CCDC #191608). For clarity, all hydrogen atoms have been omitted. Displacement ellipsoids are drawn at 50% probability.

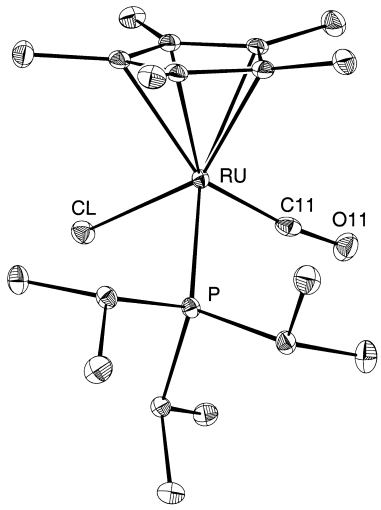

Figure 5.16: Structure of Cp*Ru(Cl)(CO)(PPr^i_3) (CCDC #183992). For clarity, all hydrogen atoms have been omitted. Displacement ellipsoids are drawn at 50% probability.

Infrared spectroscopy. The data in Table 5.4 show that the carbonyl stretching frequencies of the entire series of Cp*Ru(Cl)(CO)(L) complexes do not show any clear trend and were not particularly useful.

Table 5.4: Carbonyl stretching frequencies of Cp*Ru(Cl)(CO)(L) complexes (KBr pellet).

Complex	ν_{CO} (cm^{-1})
Cp*Ru(Cl)(CO)(Cl_2IMes)	1922
Cp*Ru(Cl)(CO)(PCy_3)	1919
Cp*Ru(Cl)(CO)(IMes)	1916
Cp*Ru(Cl)(CO)(PPr^i_3)	1914
Cp*Ru(Cl)(CO)(H_2IMes)	1911
Cp*Ru(Cl)(CO)($Pr^i_2Me_2$Im)	1906

Photoelectron spectroscopy.[30] In order to probe the electronic differences between saturated and unsaturated NHC ligands, using 1,3-dimesityl-imidazoline-2-ylidene (IMes)[40] and 1,3-dimesityl-imidazolidine-2-ylidene (H_2IMes)[41] as specific examples, These free NHCs and their Cp*Ru(Cl)(L) complexes were examined by gas-phase photoelectron spectroscopy (Figure 5.17).

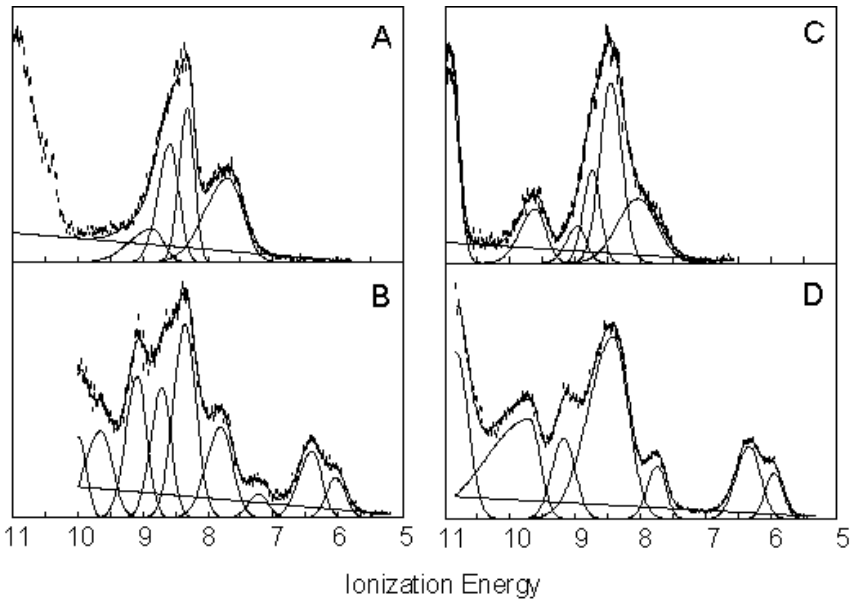

Figure 5.17: He I photoelectron spectra of H_2IMes (**A**), Cp*Ru(Cl)(H_2IMes) (**B**), IMes (**C**) and Cp*Ru(Cl)(IMes) (**D**).

40. Arduengo, A. J.; Dias, H. V. R.; Harlow, R. L.; Kline, M. *J. Am. Chem. Soc.* **1992**, *114*, 5530-5534.
41. Arduengo, A. J.; Goerlich, J. R.; Marshall, W. J. *J. Am. Chem. Soc.* **1995**, *117*, 11027-11028.

Previous photoelectron experiments by Arduengo and coworkers on 1,3-di-tert-butylimidazol-2-ylidene showed that the highest occupied molecular orbital (HOMO) was the in-plane lone pair of electrons at the carbene carbon. Other ionizations from this molecule that have been assigned include the two π-type ionizations from the NHC ring, designated π1 and π2 below.

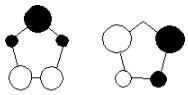

π1 π2

The ionizations present in the photoelectron spectrum of H_2IMes (Figure 5.17 **A**) can be assigned as the σ lone pair on the carbene carbon located at 7.69 eV with ionizations from the mesityl groups dominating the region between 8.3 and 8.6 eV. The spectrum for IMes free ligand (Figure 5.17 **C**) shows more structure corresponding to the π system in the imidazole ring. The carbene carbon lone pair is the HOMO and is located at 8.03 eV, with the π1 and mesityl ionizations located between 8.4 and 9.0 eV. The π2 ionization, which is stabilized relative to the π1 ionization, is located at 9.61 eV.

In this study, we are primarily interested in the bonding of unsaturated and saturated NHCs as metal-coordinated ligands. The photoelectron spectra for Cp*Ru(Cl)(L) where L = H_2IMes and IMes (Figure 5.17, **B** and **D**) show the d^6 metal ionizations occurring in a 1:2 intensity ratio. The metal ionizations for the complex where L = IMes occur at 5.95 eV and 6.33 eV, whereas the metal ionizations for the H_2IMes complex occur at 6.04 eV and 6.40 eV. Upon coordination of the NHC ligand to the metal center, the carbene sigma lone pair (HOMO in the free ligand) is stabilized, as well as both π1 and π2 ionizations.

The first ionization is a measure of the electron density at the metal center, which correlates with the overall σ-donor strength of L. In these Cp*Ru(Cl)(L) complexes, the first ionization for the IMes derivative is destabilized by 0.09 ± 0.02 eV compared to the H_2IMes derivative. This difference indicates that IMes is a slightly stronger σ-donor ligand than H_2IMes. These results are consistent with a PES study on a pair of $(CO)_4Fe(L)$ complexes, in which L = 1,3-dimethyl-imidazoline-2-ylidene was found to be a slightly stronger σ donor (by 0.1 eV) than the saturated analog 1,3-dimethyl-imidazolidine-2-ylidene.[42]

---

42. Böhm, M. C.; Daub, J.; Gleiter, R.; Hofmann, P.; Lappert, M. F.; Öfele, K. *Chem. Ber.* **1980**, *113*, 3629-3646.

III. Implications for ruthenium-catalyzed olefin metathesis

Complexes with IMes and H_2IMes ligands have been used in many catalytic processes, including hydroformylation and various cross-coupling reactions, but we are particularly interested in their applications to the olefin metathesis reaction. The ruthenium alkylidene derivatives (IMes)(PCy_3)$(Cl)_2$Ru=CHPh (**5.3**) and (H_2IMes)(PCy_3)$(Cl)_2$Ru=CHPh (**5.2**) are both highly-active olefin metathesis catalysts, but these two complexes exhibit subtle differences in *(i)* overall olefin metathesis activity (the H_2IMes derivative is slightly more active than the IMes derivative),[43,44] *(ii)* rates of phosphine dissociation and thus catalyst initiation (the H_2IMes derivative initiates faster than the IMes derivative),[45] *(iii)* barriers to Ru–NHC rotation (the barrier is larger for the H_2IMes derivative than the IMes derivative),[46] and (*iv*) k_{-1}/k_2 ratios (the H_2IMes derivative has a more favorable ratio than the IMes derivative).[45]

First and foremost, the study on $(CO)_5$Mo(L) complexes in Part I clearly showed that the NHC ligand is a superior σ-donor ligand compared even to PCy_3. However, the results also indicated that PCy_3 has some π-backbonding capabilities, whereas the NHC has none. On this basis, it is reasonable to propose that the large increase in catalytic activity in going from the bis(phosphine) derivative $(PCy_3)_2(Cl)_2$Ru=CHPh (**5.1**) to **5.2** is due to the much greater electron density of the ruthenium center in **5.2**. This property also causes an increase in the Ru→PCy_3 π backbonding, which slows down the rate of phosphine dissociation and catalyst initiation. Furthermore, the study on Cp*Ru(Cl)(L) complexes in Part II clearly showed that the IMes ligand is a slightly stronger σ-donor ligand compared to H_2IMes. This property would make the ruthenium center in **5.3** slightly more electron rich than that in **5.2** and ultimately cause slightly slower catalyst initiation.

Interestingly, Cavallo has calculated (by DFT) that the gas-phase binding energy of the Ru–NHC bond in **5.3** is greater than that in **5.2** by 5.2 kcal mol^{-1}.[47] He attributes this difference to the stabilization of the HOMO by approximately 0.15 eV in the IMes case, which is consistent with the trend observed by PES.

---

43. Examples: (a) Trnka, T. M.; Morgan, J. P.; Sanford, M. S.; Wilhelm, T. E.; Scholl, M.; Choi, T.-L.; Ding, S.; Day, M. W.; Grubbs, R. H. *J. Am. Chem. Soc.* **2002**, in press. (b) Schramm, M. P.; Reddy, D. S.; Kozmin, S. A. *Angew. Chem., Int. Ed.* **2001**, *40*, 4274-4277.
44. Also, the $[RuCl_2(p\text{-cymene})]_2$ + $[H_2IMes(H)][Cl]$ + 2 Cs_2CO_3 catalyst system for enyne metathesis is more active than the analogous [IMes(H)][Cl] system. Sémeril, D.; Cléran, M.; Bruneau, C.; Dixneuf, P. H. *Adv. Synth. Cat.* **2001**, *343*, 184-187.
45. Love, J. A.; Grubbs, R. H. **2001**, unpublished results.
46. Sanford, M. S.; Trnka, T. M.; Grubbs, R. H. **2001**, unpublished results.
47. Cavallo, L. *J. Am. Chem. Soc.* **2002**, *124*, 8965-8973.

These findings may also help explain why the reaction of [IMes(H)][Cl] with $KOBu^t$ results in deprotonation, whereas the reaction of [H_2IMes(H)][Cl] with $KOBu^t$ results in H_2IMes(H)(OBu^t) adduct formation: because IMes is a slightly stronger σ-donor, [IMes(H)][Cl] is should be easier to deprotonate than [H_2IMes(H)][Cl]. The deprotonation of [H_2IMes(H)][Cl] can be accomplished with stronger bases, such as KH.

Experimental

General considerations: All manipulations involving organometallic complexes were performed using a combination of glovebox, high vacuum, and Schlenk techniques under a nitrogen atmosphere, unless otherwise specified. Solvents were dried and degassed by standard procedures. NMR spectra were obtained on Varian Inova 500 and Mercury 300 spectrometers. ^{1}H NMR chemical shifts are reported in ppm relative to $SiMe_4$ ($\delta = 0$) and referenced internally with respect to the protio solvent impurity. ^{13}C NMR spectra were referenced internally with respect to the solvent resonance. ^{31}P NMR spectra were referenced using H_3PO_4 ($\delta = 0$) as an external standard. ^{19}F NMR spectra were referenced using CCl_3F ($\delta = 0$) as an external standard. ^{95}Mo NMR spectra (26.01 MHz) were measured on a JEOL JNM-GX400 spectrometer; they were referenced externally with respect to Na_2MoO_4 in D_2O ($\delta = 0$) and internally with respect to added $(CO)_6Mo$ ($\delta = -1857$). Coupling constants are in hertz. IR spectra were recorded on a Perkin-Elmer Paragon 1000 spectrophotometer; the data are reported in reciprocal centimeters. Elemental analyses were measured by Midwest Microlab, Indianapolis, IN. Mass spectral analysis was performed at the Southern California Mass Spectrometry Facility (University of California at Riverside). Silica gel for the purification of organometallic complexes was obtained from TSI Scientific, Cambridge, MA (60 Å, pH 6.5-7.0).

Crystallographic data (excluding structure factors) for the structures in this chapter have been deposited with the Cambridge Crystallographic Data Centre. Deposition numbers are included in the figure captions. These data can be obtained free of charge via http://www.ccdc.cam.ac.uk/conts/retrieving.html (or by e-mail: deposit@ccdc.cam.ac.uk). Structure factors are also available by e-mail (xray@caltech.edu).

Characterization of $(CO)_5Mo(NMe_3)$: This compound was synthesized by the method in reference 26. ^{1}H NMR (C_6D_6): δ 1.80 (s, 9H, Me). $^{13}C\{^{1}H\}$ NMR (C_6D_6): δ 59.17 (s, Me), 204.65 (s, CO_{eq}), 214.30 (s, CO_{ax}). Crystals for x-ray analysis were grown by cooling a hexanes solution of $(CO)_5Mo(NMe_3)$ at –10°C.

Synthesis and characterization of $(CO)_5Mo(PCy_3)$: 0.276 g of $(CO)_5Mo(NMe_3)$ (0.935 mmol) and 0.288 g of PCy_3 (1.029 mmol, 1.1 eq) were dissolved in 20 mL benzene and stirred for 12 hrs at room temperature. The reaction mixture was filtered and the supernatant pumped down

under vacuum. The resulting material was redissolved in a minimum amount of hexanes and cooled at –10°C to provide 0.25 g of $(CO)_5Mo(PCy_3)$ as pale yellow crystals (52% yield). ^1H NMR (C_6D_6): δ 1.07 (m, 6H, Cy), 1.29 (m, 6H, Cy), 1.53 (br s, 3H, Cy), 1.63 (m, 6H, Cy), 1.73 (m, 6H, Cy), 1.81 (br d, J_{HP} = 12 Hz, 6H, Cy). $^{13}C\{^1H\}$ NMR (C_6D_6): δ 26.80 (s, Cy), 28.04 (m, Cy), 30.60 (d, J_{CP} = 5, Cy), 36.62 (d, J_{CP} = 13, Cy), 208.32 (s, CO_{eq}), 210.85 (s, CO_{ax}). Anal. Calcd. for $C_{23}H_{33}PO_5Mo$: C, 53.49%; H, 6.44%. Found: C, 53.98%; H, 6.59%.

Characterization of $(CO)_5Mo(Pr^i_2Me_2Im)$: ^1H NMR (C_6D_6): δ 1.10 (d, J = 7, 12H, Pr^i Me), 1.65 (s, 6H, backbone Me), 5.56 (septet, J = 7, 2H, Pr^i CH). $^{13}C\{^1H\}$ NMR (C_6D_6): δ 10.60 (s, backbone Me), 21.83 (s, Pr^i Me), 55.01 (s, Pr^i CH), 126.92 (s, C=C), 207.01 (s, CO_{eq}), 213.20 (s, CO_{ax}), 185.36 (s, NCN).

Characterization of $(CO)_5Mo(H_2IMes)$: ^1H NMR: 2.12 (s, 6H, *p*-Me of Mes), 2.17 (s, 12H, *o*-Me of Mes), 3.00 (s, 4H, CH_2CH_2), 6.78 (s, 2H, *m*-H of Mes). ^{13}C NMR: 17.79 (*o*-Me of Mes), 21.00 (*p*-Me of Mes), 51.00 (CH_2CH_2), 130.21 (Mes), 136.20 (Mes), 138.53 (Mes), 138.88 (Mes), 205.98 (eq CO), 211.69 (ax CO), 221.98 (CN_2).

Photoelectron spectroscopy: The photoelectron spectra were recorded using a McPherson ESCA36 instrument that features a 36 cm radius, 8 cm gap hemispherical analyzer and custom designed sample cells and detection and control electronics. The excitation source was a quartz lamp that produced both He I and He II radiation, depending on the operating conditions. The argon $^2P_{3/2}$ ionization at 15.759 eV was used as an internal calibration lock of the absolute ionization energy. The difference between the argon $^2P_{3/2}$ and the methyl iodide $^2E_{1/2}$ ionization at 9.538 eV was used to calibrate the ionization energy scale. During data collection the instrument resolution, measured using the full width at half-maximum of the argon $^2P_{3/2}$ ionization, was 0.020-0.030 eV. All data are intensity corrected with an experimentally determined instrument analyzer sensitivity function that assumes a linear dependence of analyzer transmission (intensity) to the kinetic energy of the electrons within the energy range of these experiments. The sublimation temperature was monitored using a "K" type thermocouple passed through a vacuum feedthrough and attached directly to the cell. The spectra were obtained for each compound within the range of the following cell temperatures: $(CO)_6Mo$, 25°C; $(CO)_5Mo(NMe_3)$, 25°C; $(CO)_5Mo(PMe_3)$, 35 ± 4°C; $(CO)_5Mo(PPh_3)$; $(CO)_5Mo(PCy_3)$, 115-

125°C; $(CO)_5Mo(Pr^i_2Me_2Im)$, 112-135°C. A custom-made aluminum sample cell was used to hold the compound.

Synthesis and characterization of Cp*Ru(Cl)(H_2IMes): A mixture of 0.130 g (0.243 mmol) $[Cp^*Ru(\mu\text{-}OMe)]_2$ and 0.300 g (0.875 mmol) [H_2IMes(H)][Cl] in 8 mL benzene was stirred at 70°C for 14 hrs. The resulting purple mixture was filtered, and the supernatant was pumped down. The product was extracted into 30 mL hexanes, which was filtered and pumped down. The resulting solid was washed with 2 mL of cold hexanes and dried under vacuum to provide 0.065 g of Cp*Ru(Cl)(H_2IMes) as a dark blue, crystalline solid (23%). More product can be obtained by cooling the hexanes wash overnight at −10°C. Anal. Calcd. for $C_{31}H_{41}N_2ClRu$: C, 64.40%; H, 7.15%; N, 4.84%. Found: C, 64.49%, H, 7.12%; N, 4.95%.

Synthesis of the IMes free carbene: Under an inert atmosphere, charge a flame-dried Schlenk flask with 1.00 g [IMes][Cl] and ~10 mL dry THF. Also under an inert atmosphere, charge another flame-dried Schlenk flask with a small piece of K (~0.75 cm^3). On a vacuum line, connect the two flasks with a transfer line. Condense ~15 mL anhydrous NH_3 into the Schlenk with the K at dry ice/acetone temperature. Then transfer the NH_3 into the other Schlenk at dry ice/acetone temperature. Under a positive pressure of inert atmosphere, add 0.072 g NaH all at once. Allow the reaction to warm to room temperature over the course of ~6 hrs (keep the reaction under a low positive pressure of inert atmosphere the whole time.) The NH_3 will evaporate, and the reaction mixture will be less cloudy and light brown in color. Pump down the mixture and extract the product with ~15 mL dry hexanes. Cool the extract at −20°C overnight and collect the yellowish crystalline material. Yield varies from 30 to 80%, depending on the NaH quality.

Table 5.5: ^{1}H, ^{31}P, and ^{13}C NMR data for Cp*Ru(Cl)(L) and Cp*Ru(Cl)(CO)(L) derivatives.

Complex (solvent)	**δ Cp***	**δ L**	**δ ^{31}P**	**δ Cp* (Me, Cp ring)**	**δ L**	**δ CO**	**δ NCN**
Cp*Ru(Cl)(PPr^{i}_3) (CD_2Cl_2)	1.51 (d, J_{HP} = 0.5 Hz)	1.16 (d, J_{HP} = 7 Hz, 9H, Me), 1.19 (d, J_{HP} = 7 Hz, 9H, Me), 2.32 (m, J_{HP} = 1.5 and 8 Hz, 3H, CH)	52.99	11.26, 74.74	16.83 (d, J_{CP} = 3 Hz, Me of PPr^{i}_3), 20.46 (d, J_{CP} = 2 Hz, Me of PPr^{i}_3), 24.45 (d, J_{CP} = 17 Hz, CH of PPr^{i}_3)	—	—
Cp*Ru(Cl)(PCy_3) (CD_2Cl_2)	1.50 (d, J_{HP} = 0.5 Hz)	1.22 (br, 9H, Cy), 1.37 (br m, 6H, Cy), 1.69 (br, 3H, Cy), 1.75 (br m, 12H, Cy), 2.09 (br quartet, 3H, Cy)	41.70	11.39, 74.58	27.17 (d, J_{CP} = 2 Hz, Cy), 28.38 (d, J_{CP} = 10 Hz, Cy), 30.84 (s, Cy), 34.31 (d, J_{CP} = 17 Hz, Cy)	—	—
Cp*Ru(Cl)($Pr^{i}_2Me_2Im$) (CD_2Cl_2)	1.59	1.13 (d, J_{HH} = 7, 6H, Pr^{i} Me), 1.56 (d, J_{HH} = 7, 6H, Pr^{i} Me), 2.15 (s, 6H, backbone Me), 4.77 (septet, J_{HH} = 7, 2H, CH)	—	11.48, 73.29	10.69 (backbone Me), 21.95 (Pr^{i} Me), 22.93 (Pr^{i} Me), 53.31 (CH), 125.36 (C=C)	—	194.58
Cp*Ru(Cl)(IMes) (CD_2Cl_2)	1.07	1.96 (br s, 6H, *o*-Me), 2.33 (s, 6H, *p*-Me), 2.43 (br s, 6H, *o*-Me), 6.91 (br s, 2H, *m*-H), 6.94 (s, 2H, backbone CH), 7.01 (br s, 2H, *m*-H)	—	10.65, 73.03	19.38 (br, Me), 19.72 (br, Me), 21.29 (s), 123.99 (C=C), 128.89 (br, Mes), 129.61 (br, Mes), 135.65 (s, Mes), 137.49 (s, Mes), 138.86 (s, Mes)	—	199.29
Cp*Ru(Cl)(H_2IMes) (THF-d_8)	1.59	2.71 (s, 6H, Me), 2.81 (s, 6H, Me), 3.28 (s, 6H, Me), 4.29 (m, 2H, CH_2CH_2), 4.45 (m, 2H, CH_2CH_2), 7.36 (*m*-H), 7.51 (*m*-H)	—	10.8, 74.4	19.5 (Me), 20.0 (Me), 21.3 (Me), 118.3 (C=C), 129.5 (Mes), 130.4 (Mes), 135.1 (Mes), 136.9 (Mes), 139.1 (Mes), 140.4 (Mes)	—	203.8
Cp*Ru(Cl)(CO)(PPr^{i}_3) (CD_2Cl_2)	1.71 (d, J_{HP} = 1.5 Hz)	1.20 (dd, J_{HP} = 7 and 12 Hz, 9H, Me), 1.26 (dd, J_{HP} = 7 and 12 Hz, 9H, Me), 2.38 (m, J_{HP} = 2 and 7 Hz, 3H, CH)	60.31	10.63 (s), 96.48 (d, J_{CP} = 2 Hz)	19.91 (d, J_{CP} = 2.5 Hz, Me of PPr^{i}_3), 20.85 (d, J_{CP} = 1 Hz, Me of PPr^{i}_3), 26.28 (d, J_{CP} = 20 Hz, CH of PPr^{i}_3)	210.12	—
Cp*Ru(Cl)(CO)($Pr^{i}_2Me_2Im$)	1.68	1.49 (br, 12H, Pr^{i} Me),	—	9.23,	9.87 (backbone Me),	207.53	178.51

(CD_2Cl_2)		2.23 (s, 6H, backbone Me), 5.32 (br, 2H, CH)		92.66	21.58 (br, Pr^i Me), 22.57 (br, Pr^i Me), 23.97 (br, Pr^i Me), 52.45 (br, CH), 127.70 (C=C)		
Cp*Ru(Cl)(CO)(IMes) (CD_2Cl_2)	1.32	2.12 (s, 6H, Me), 2.20 (s, 6H, Me), 2.36 (s, 6H, Me), 6.86 (s, 2H, backbone CH), 6.99 (m, 2H, *m*-H), 7.01 (m, 2H, *m*-H)	—	9.92, 93.94	19.07 (Me), 19.49 (Me), 21.37 (Me), 124.91 (CH_2CH_2), 129.69 (Mes), 129.83 (Mes), 137.54 (Mes), 137.80 (Mes), 139.15 (Mes), 139.55 (Mes)	207.87	186.44